Fabrication and Deodorizing Efficiency of Nanostructured Core-Sheath TiO_2 Nanofibers

Soonjee Park,[1] Hae-Rim Kim,[2] Hyunsik Bang,[2] Kazushige Fujimori,[2] Byoung-Suhk Kim,[2] Soon-Ho Kim,[3] Ick-Soo Kim[2]

[1]*School of Textiles, Yeungnam University, Gyeongsan, Gyeongbuk 712-149, Republic of Korea*
[2]*Nano Fusion Technology Research Laboratory, Faculty of Textile Science and Technology, Shinshu University, Ueda, Nagano 386-8567, Japan*
[3]*Department of Automotive Mechanical Engineering, College of Engineering, Silla University, Busan 617-736, Korea*

Received 8 June 2011; accepted 16 November 2011
DOI 10.1002/app.36499
Published online 31 January 2012 in Wiley Online Library (wileyonlinelibrary.com).

ABSTRACT: In this work, we report the fabrication and deodorizing efficiency of nanostructured core-sheath TiO_2 nanofibers prepared by a combined technique of electrospinning and metallization. The morphologies and crystal structures of the resultant nanofibers were investigated by emission scanning electron microscopy (SEM), transmission electron microscopy (TEM), and wide angle X-ray diffraction (WAXD), respectively. The influence of annealing conditions, such as annealing temperature and time, various titanium isopropoxide (TTIP) weight fractions, which are based on the weight of the poly(vinyl acetate) (PVAc), on morphologies and crystal structures was evaluated for the nanostructured core-sheath TiO_2 nanofibers. UV blocking properties and deodorizing efficiency were also measured by UV-visible spectrometer and formaldehyde detector tube at room temperature, respectively. © 2012 Wiley Periodicals, Inc. J Appl Polym Sci 125: 2929–2935, 2012

Key words: fibers; annealing; microstructure; structure–property relations; nanotechnology

INTRODUCTION

In the last few decades, a huge interest in the field of nanofibers has appeared because of their excellent properties and wide variety of potential applications. Polymer nanofibers have unique and interesting features such as a high surface area to volume ratio, flexibility in terms of surface functionalities, and good mechanical performance, and therefore they can be employed in a large range of applications such as textiles, filters, catalysis, artificial tissue scaffolds, porous electrodes, biomaterials, electronics, and composite reinforcement.[1–5]

Titanium dioxide (TiO_2) has been widely used as a material in the wide band-gap, semiconductive, ceramic, solar cell, and photocatalysis.[6–10] In general, TiO_2 has two common crystalline forms: the rutile and the anatase forms. The rutile TiO_2 has a tetragonal crystalline structure, while the anatase TiO_2 has an octahedral crystalline structure. Particularly, the anatase TiO_2 exhibits higher activities for the solar cell and photocatalysis applications.[11,12] The photocatalyst has various characters. A typical character is an extremely high oxidizing power by hydroxy radical. The hydroxy radical is able to cut easily the atomic bond of an organic compound. The harmful materials are not absorbed but are resolved to the harmless materials by photocatalyst. Therefore, photocatalyst has a great potential for a wide range of applications in many industries, such as deodorizing, countermeasure of sick building syndrome, changing nitrogen and sulfur oxides to nitrate salt and hydrosulfate, resolving dioxin to H_2O, CO_2, and chlorine ion, purification of drain and soil contamination, bacterial killing, and so on.[13–15] Ramakrishna et al.[16] developed the anatase TiO_2 nanofibers of average diameters 60, 100, and 150 nm via controlled electrospinning of a polymeric solution and subsequent sintering of the as-spun fibers composed of densely TiO_2 grains of size $\sim$ 12 nm. Tuller et al.[17] reported that electrospun TiO_2 nanofiber mats exhibited exceptional sensitivity to NO_2 with a detection limit estimated to be well below 1 ppb.

Polymeric nanofibers with core-shell structure have been attracting special attention in the past decade for the unique properties which could potentially be applied in the areas of catalysis, optical and electronical devices, and biomaterials.[18–20] So far, several methods have been developed to prepare core-shell structure of polymeric nanofibers by electrospinning. For instance, Kumar et al.[21] reported the fabrication

Correspondence to: B. S. Kim (kbsuhk@yahoo.com) and I. S. Kim (kim@shinshu-u.ac.jp).

of novel metal oxide-coated polymeric nanofibers using the electrospinning and solution dipping technique. Greiner et al.[22] reported that the coating of the template and the formation of the walls of the tubes could be achieved by chemical vapor deposition (CVD) with poly(*p*-xylylene) (PPX) via a template route. In our previous article,[23,24] we reported that metallized conductive nanofibers can be successfully prepared by using a combined technique of electrospinning and metallization, which makes it possible easily to modify surface properties of electrospun nanofibers. For instance, Cu-metallized nanofibers showed enhanced surface conductivity and higher mechanical properties.[23] Furthermore, by this technique, the functional component could be encapsulated as the core or coated as the shell. In this work, we prepared the core-sheath TiO_2 nanofibers by using the same combined technique of electrospinning and metallization, and investigated UV blocking and deodorizing efficiency, respectively.

EXPERIMENTAL

Materials

Poly(vinyl acetate) (PVAc) ($M_w \sim$ 500,000 g/mol) was obtained from Celanese. Titanium isopropoxide (TTIP), *N*,*N*-dimethylformamide (DMF), ethanol (EtOH), and acetic acid (99 wt %) were purchased from Wako Japan, and used as received without further purification.

Electrospinning and metallization

A high-voltage power supply (Har-100*12, Matsusada, Tokyo, Japan) was used to generate high voltage of 10 kV. The polymer solutions were supplied through a plastic syringe attached to a capillary tip with an inner diameter of 0.6 mm.[2–5,23–27] The copper wire connected to a positive electrode (anode) was inserted into the polymer solution, and a negative electrode (cathode) was attached to a metallic collector. The high potential electrode of the power supply was connected to a copper wire inserted into the solution, and the ground electrode to the metallic collector which is a rotating metallic drum wrapped with Al-foil. Nonwoven fibrous PVAc mats were collected on the surface of Al-foil that was covered on the grounded collector. The PVAc was dissolved in the mixed solvents of DMF and EtOH (DMF/EtOH = 80/20, w/w) at a concentration of 18 wt %, and then mixed with TTIP and acetic acid under vigorous stirring. After stirring for 1 h, the solution was used for electrospinning.

A system UEP-6000 (ULVAC, Japan) was used to deposit a metal layer on the nonwoven mats. A high-purity titanium was mounted on the vapor plate, and the nanofiber mats were fixed on the rotating holder with a side facing the target. The vacuum pressure was set at 8.0×10^{-3} Pa, the power set at 10 kV, 40 mA. The distance between the target and the substrates was fixed at 400 nm, and the deposition rate of the metallic layer was controlled to be about 0.1 nm/s. All depositions were performed on both sides of the nanofiber mats. To produce the metallic nanofibers, the metal-deposited nonwoven nanofiber mats were calcined at 400, 600, and 900°C in air for 10 h. The heating rate was 5.0°C/min.

Characterization

Solution properties, such as viscosity and surface tension, were measured with a Brookfield digital viscometer (Model DV-E) and surface tensiometer (Kruss Model K8) at room temperature, respectively. The morphologies were characterized by field emission scanning electron microscopy (FE-SEM) (Hitachi model S-5000) and transmission electron microscopy (TEM) (JEOL model 2010 FasTEM, accelerating voltage 200 kV), respectively. Wide angle X-ray diffraction (WAXD) experiments were carried out with a fixed anode X-ray generator operating at 40 kV and 150 mA (Rotaflex RTP300, Rigaku, Japan). The UV blocking ability was evaluated by using a UV-visible spectrometer (Lambda 900, Perkin-Elmer, USA) in the 200–600 nm range. The deodorizing experiment was carried out at room temperature as follows. First, we produced the deodorized gas by heating the formaldehyde so that the concentration of formaldehyde gas was about 300 ppm in the test chamber (64 l). The formaldehyde gas in the test chamber was fan-stirred for 3 min. Afterwards, the formaldehyde gas in the test chamber was extracted by using 100-mL injection syringe and injected into desiccator with sample. And then, formaldehyde gas in the chamber was again fan-stirred for 3 min. In this work, the gas concentration in desiccator was 5.0 ± 0.5 ppm. After injecting the formaldehyde gas, the desiccator was then irradiated with UV light. The gas concentration was measured by formaldehyde detector tube (GV-100s, GASTEC Co., Japan) at an interval of 10 min for about 40 min. The decrease ratio (%, deodorizing efficiency) was calculated as $[(C_i - C_t)/C_i] \times 100\%$, where C_i and C_t are the formaldehyde gas concentration at the initial and elapsed times, respectively. We used Pt heater as a heating gas. A regulated DC power supply (PAN 16-10A, KKUSU, Japan) was used to generate high voltage of 10 V. The size of nonwoven nanofibers and films were 50 mm × 40 mm (length × width), respectively. Figure 1 shows the experimental apparatus for measuring gas sensitivity.

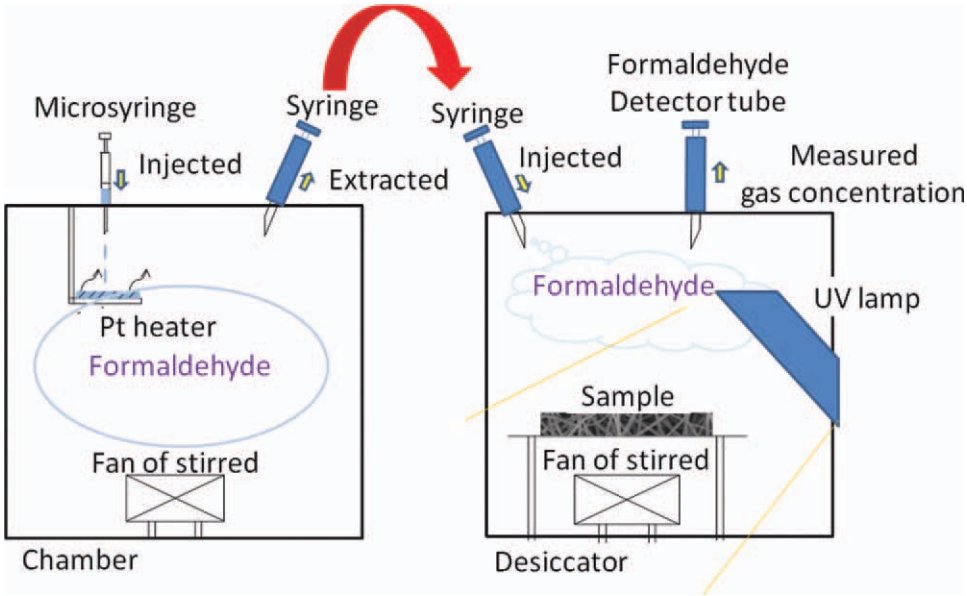

Figure 1 Experimental apparatus for measuring gas sensitivity. [Color figure can be viewed in the online issue, which is available at wileyonlinelibrary.com.]

RESULTS AND DISCUSSION

Solution properties and electrospinning of PVAc/TTIP blends

In general, solution properties, such as viscosity, surface tension, determine the limited boundaries for the formation of electrospun fibers by solution electrospinning. In this work, the PVAc solutions with various TTIP weight fractions (φ_{TTIP}) ranging from 0.1 to 0.8 were used for solution electrospinning. The concentration of the PVAc solution dissolved in the mixed solvents of DMF and EtOH (DMF/EtOH = 80/20, w/w) was about 18 wt %. Figure 2 shows SEM images and average fiber diameter of PVAc/TTIP nanofibers electrospun from the PVAc solutions in terms of various φ_{TTIP}.

As seen in Figure 2, all PVAc/TTIP solutions produced the nanofibers. The average diameter of PVAc/TTIP nanofibers at $\varphi_{TTIP} = 0.1$ slightly decreased due to the decreased solution viscosity (see Table I), which was made by mixing TTIP and acetic acid (as a cosolvent) with PVAc solution. Moreover, the smaller fiber diameter as well as the narrower fiber diameter distribution were observed at $\varphi_{TTIP} = 0.1$. As φ_{TTIP} increased further, the distribution of fiber diameter became larger although no change in fiber diameter was detected up to $\varphi_{TTIP} = 0.6$. The murky white phenomenon was observed when φ_{TTIP} increased over $\varphi_{TTIP} = 0.2$. On the other hand, above $\varphi_{TTIP} = 0.8$ the murky white phenomenon was intensified and the spinning ability got worse. The amount of the deposited electrospun fibers was decreased, and the drops of solution and nozzle clogging were often observed. Accordingly, the fiber diameter increased. From these results, it was concluded that the optimum φ_{TTIP} condition for PVAc/TTIP electrospinning was 0.2.

Morphologies of Ti-deposited TiO_2 nanofibers

Figure 3 shows SEM images of pure PVAc nanofibers (a), PVAc/TTIP nanofibers ($\varphi_{TTIP} = 0.2$) (b), 100 nm (c) and 200 nm (d) Ti-deposited PVAc/TTIP ($\varphi_{TTIP} = 0.2$) nanofibers. The average fiber diameter of pure PVAc nanofibers was ca. 1560 nm, whereas PVAc/TTIP nanofibers ($\varphi_{TTIP} = 0.2$) showed smaller fiber diameter of ca. 330 nm. This might be derived from the decreased viscosity and increased conductivity by added TTIP into PVAc solution. After metal deposition onto both sides of nanofiber webs, average fiber diameter of 100 and 200 nm Ti-deposited PVAc/TTIP nanofibers were found to be ca. 530 nm and ca. 740 nm, indicating a successful Ti metal deposition.

Figure 4 shows SEM images of Ti-deposited TiO_2 nanofibers ($\varphi_{TTIP} = 0.2$), which were obtained after annealing of both 100 and 200 nm Ti-deposited PVAc/TTIP nanofibers at 400, 600, 900°C for 10 h, respectively. Importantly, the fibrous morphologies were satisfactorily conserved even after removal of the nanofiber template through an annealing process, suggesting the successful deposition of metallic layers onto the surface of the nanofiber template. Moreover, the metal-deposited nanofibers exhibited a rough surface morphology,[23] compared with pure PVAc and PVAc/TTIP nanofibers. Furthermore, the irregular-shaped nanoparticles were converged gradually and its size became larger as increasing the annealing temperature, which may be attributed to

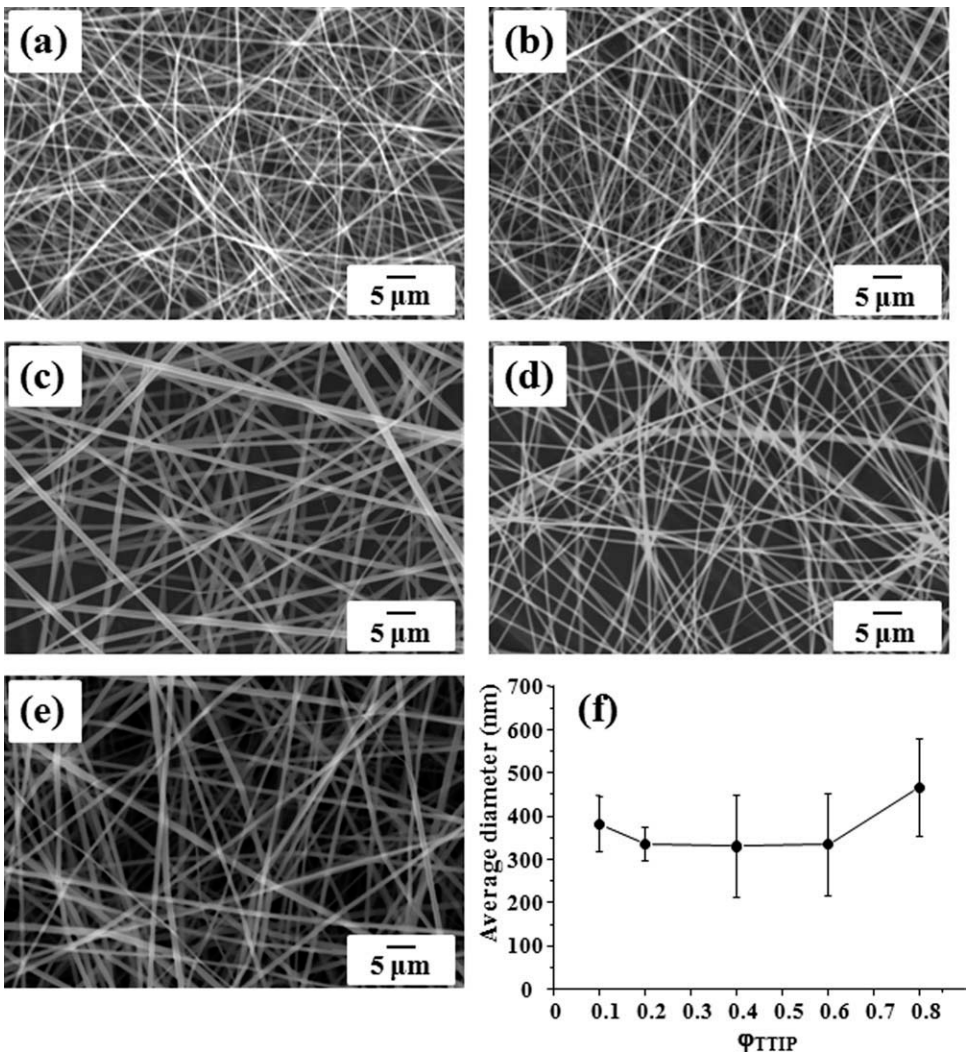

Figure 2 SEM images and average fiber diameters of PVAc/TTIP nanofibers electrospun from the PVAc solutions with various φ_{TTIP}. The concentration of the PVAc solution dissolved in the mixed solvents of DMF and EtOH (DMF/EtOH = 80/20, w/w) was about 18 wt %.

the massive metal migration and aggregation during annealing at higher temperature. The result is well in accordance with the previously reported paper,[23,24] and was also confirmed by FE-SEM (Fig. 4) and TEM (Fig. 5) analysis.

Figure 5 shows TEM images of Ti-deposited TiO_2 nanofibers annealed at different temperatures for 10 h. Particularly, unique core-sheath structures were observed after annealing at 400 and 600°C. The particle sizes in both core and sheath parts became dramatically larger, for instance, from ca. 10 nm to ca. 220 nm after annealing at 600°C. After annealing at temperature = 900°C, the particle size further increased to ca. 280 nm, which was bigger than those of two different samples annealed at 400 and 600°C, respectively, suggesting a crystal transformation from anatase to rutile type, as confirmed by XRD analysis, which will be explained later. Moreover, no core-sheath structures were detected.

TABLE I
Viscosity and Surface Tension of PVAc/TTIP Solutions in Terms of Various TTIP Weight Fractions (φ_{TTIP})

φ_{TTIP} (w/w)	Viscosity (cP)	Surface tension (m*N*/m)
0.1	749.8	31.3
0.2	659.9	31.0
0.4	331.1	29.5
0.6	256.7	27.0
0.8	184.8	-

The temperature was at about 25°C.

Crystal structures of Ti-deposited TiO_2 nanofibers

Figure 6 shows WAXD patterns of Ti-deposited PVAc/TTIP nanofibers before annealing (a) and Ti-deposited TiO_2 nanofibers annealed at 400°C (b), 600°C (c), and 900°C (d) for 10 h. As seen in Figure 6, Ti-deposited TiO_2 nanofibers annealed at 400°C clearly exhibited typical peak at $2\theta = 25.3°$,

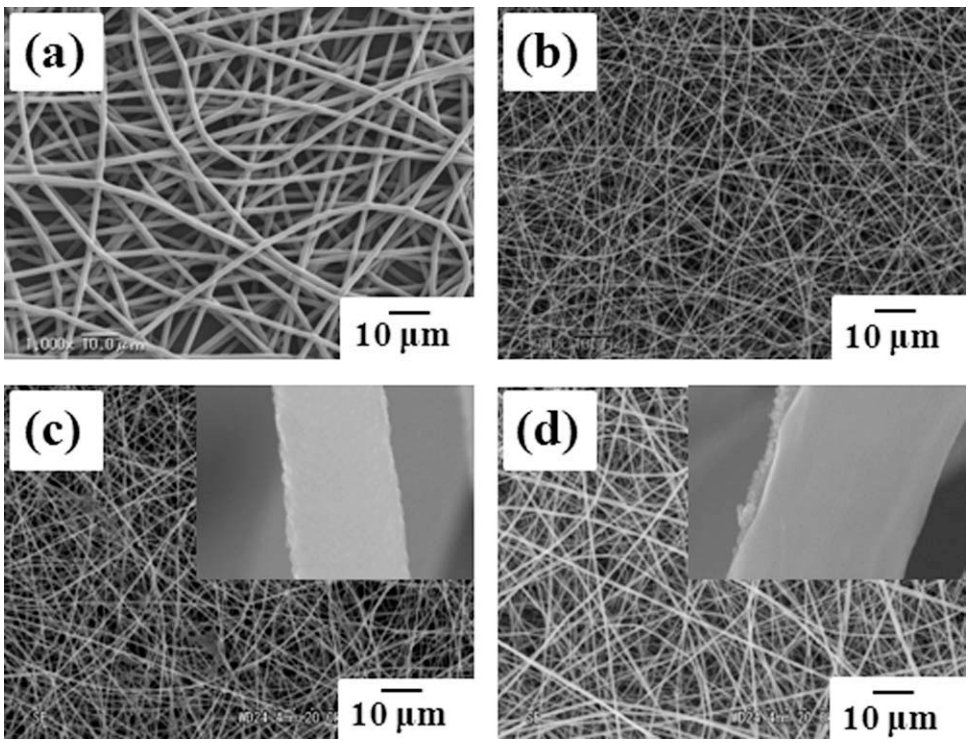

Figure 3 SEM images of pure PVAc nanofibers (a), PVAc/TTIP nanofibers ($\varphi_{TTIP} = 0.2$) (b), 100 nm (c) and 200 nm (d) Ti-deposited PVAc/TTIP ($\varphi_{TTIP} = 0.2$) nanofibers.

corresponding to the (101) reflection of TiO_2 anatase crystals,[28] while interestingly the same sample annealed at 600°C showed new peaks appearing at $2\theta = 25.4°$, 38.0°, 48.0°, 55.0°, and 62.0°, which correspond to the (101), (004), (200), (211), and (204) reflections, indicating the formation of TiO_2 rutile crystals. On the other hand, in case of the same sample annealed at 900°C, the crystal peaks corresponding to

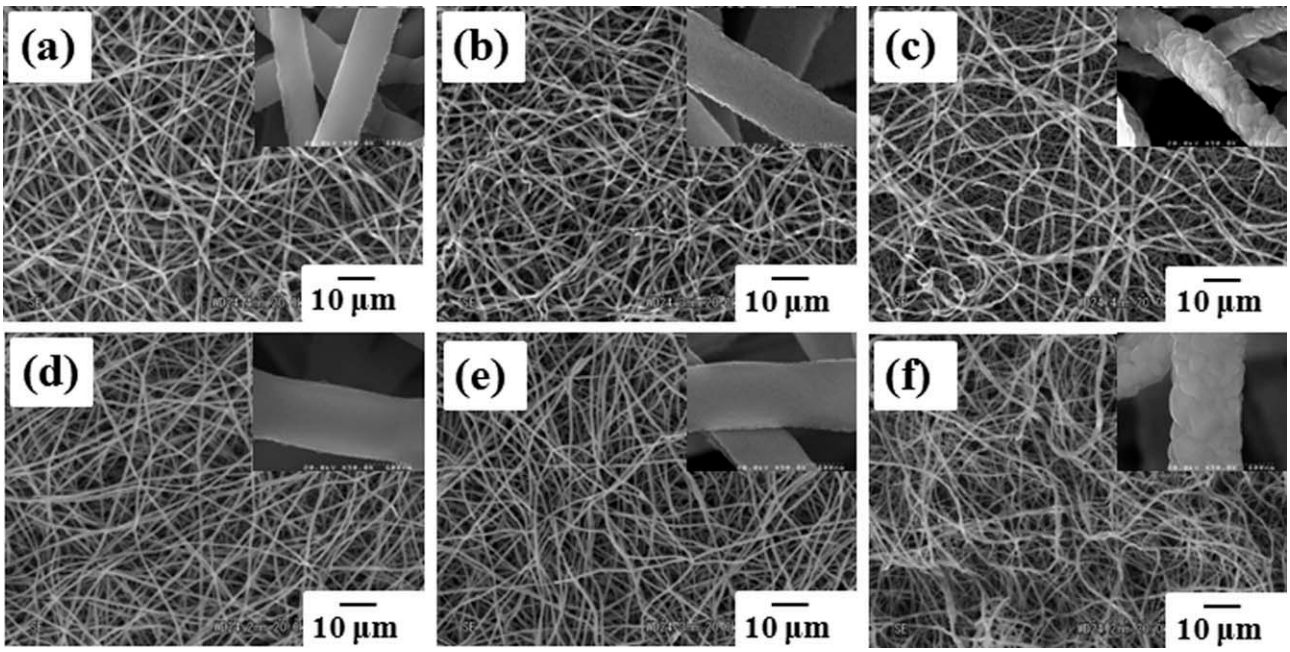

Figure 4 SEM images of Ti-deposited TiO_2 nanofibers ($\varphi_{TTIP} = 0.2$). Top: 100 nm Ti-deposited PVAc/TTIP nanofibers annealed at 400°C (a), 600°C (b), 900°C (c) for 10 h, bottom: 200 nm Ti-deposited PVAc/TTIP nanofibers annealed at 400°C (d), 600°C (e), 900°C (f) for 10 h, respectively. Insets show FE-SEM images of each nanofibrous webs at higher magnification.

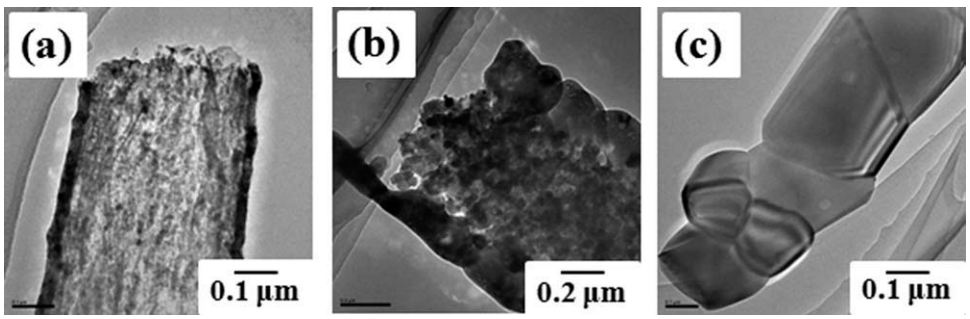

Figure 5 TEM images of Ti-deposited TiO_2 nanofibers annealed at 400°C (a), 600°C (b), and 900°C (c) for 10 h. The thickness of deposited Ti metal is 100 nm.

TiO_2 anatase were disappeared. In contrast, TiO_2 rutile crystal peaks became significantly evident, suggesting the transformation of TiO_2 anatase into TiO_2 rutile crystals. In addition, three characteristic peaks at $2\theta = 37.2^\circ$, 43.2°, and 62.9° were also observed, corresponding to the (111), (200), and (220) reflections of NiO crystalline peaks.[29] The similar microstructures were also observed for 200 nm Ti-deposited TiO_2 nanofibers depending on annealing temperature.

UV spectra analysis

To investigate the UV blocking properties of Ti-deposited TiO_2 nanofibers, the UV-visible spectra of each sample were measured at room temperature. Figure 7 shows UV-visible spectra of Ti-deposited TiO_2 nanofibers annealed at 400, 600, and 900°C. It was clearly seen that the transmission below 350 nm was considerably lower than 10%, suggesting good reflection or absorption features as an excellent ultraviolet blocking capacity. Particularly, Ti-deposited TiO_2 nanofibers annealed at 400°C showed lowest transmission value. This derives from the fact that anatase-type has the most outstanding property as a photocatalysis.

Deodorizing efficiency

Photocatalytic degradation of formaldehyde gas was used to evaluate the photocatalytic activities of Ti-deposited TiO_2 nanofibers. Figure 8 shows the results of photocatalytic degradation of formaldehyde gas by Ti-deposited TiO_2 nanofibers (Ti thickness ~ 100 nm) annealed at different temperatures. The photodegradation test of formaldehyde gas was measured every 10 min under UV irradiation. Compared to background without the specimens, Ti-deposited TiO_2 nanofibers annealed at 400 and 900°C exhibited higher deodorizing efficiency, as seen in Figure 8. Although background itself showed deodorizing efficiency of about 37.8% at 40 min,

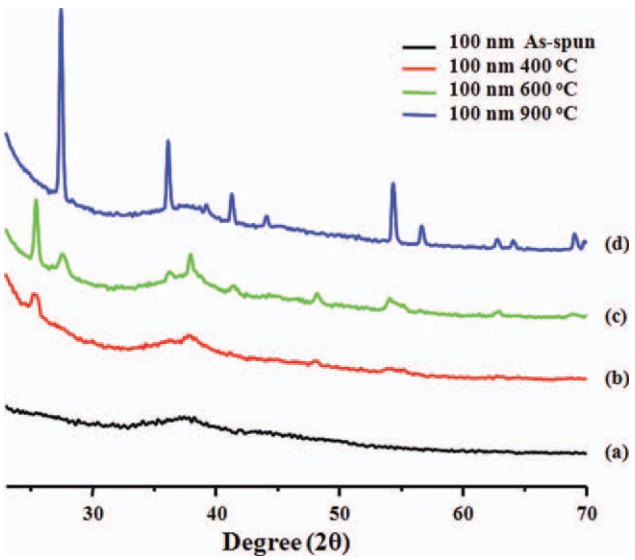

Figure 6 XRD patterns of Ti-deposited PVAc/TTIP nanofibers before annealing (a) and after annealing at 400°C (b), 600°C (c), and 900°C (d) for 10 h. The thickness of deposited Ti metal is 100 nm. [Color figure can be viewed in the online issue, which is available at wileyonlinelibrary.com.]

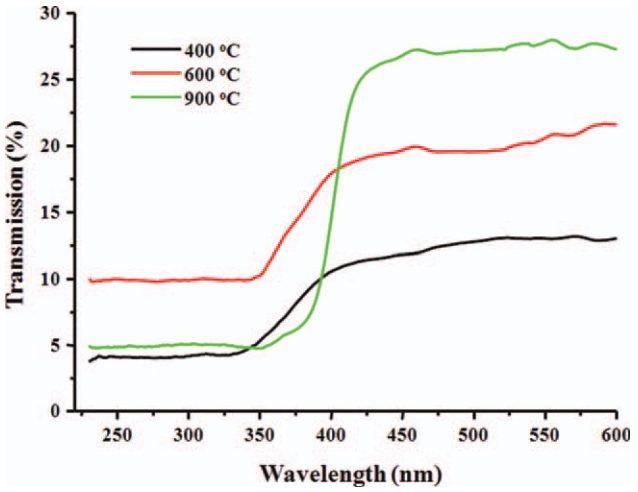

Figure 7 UV-visible spectra of Ti-deposited TiO_2 nanofibers annealed at 400, 600, and 900°C. The thickness of deposited Ti metal is 100 nm. [Color figure can be viewed in the online issue, which is available at wileyonlinelibrary.com.]

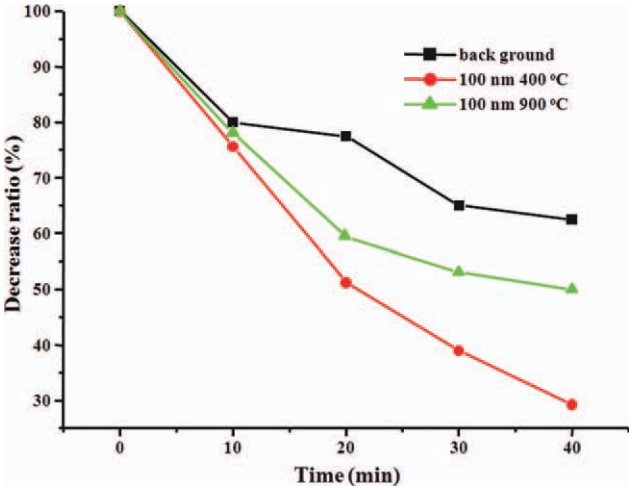

Figure 8 Photocatalytic degradation of formaldehyde gas by Ti-deposited TiO_2 nanofibers annealed at different temperatures (400 and 900°C) at room temperature. [Color figure can be viewed in the online issue, which is available at wileyonlinelibrary.com.]

probably due to inevitably decreased concentration of formaldehyde gas during the test, Ti-deposited TiO_2 nanofibers annealed at 400°C clearly showed dramatic decrease in formaldehyde gas (deodorizing efficiency ~ 70.7%), which is obviously higher than that (deodorizing efficiency ~ 50.0%) of the same sample annealed at 900°C, indicating that anatase type has more effective photocatalysis performance than rutile type.

CONCLUSIONS

In conclusion, we have successfully prepared the nanostructured core-sheath TiO_2 nanofibers prepared by using a combined technique of electrospinning and metallization. SEM analysis demonstrated that the smaller fiber diameter as well as the narrower distribution of the fiber diameter was observed at $\varphi_{TTIP} = 0.1$. As φ_{TTIP} increased further, the distribution of the fiber diameter became larger although no change in fiber diameter was detected up to $\varphi_{TTIP} = 0.6$. Above $\varphi_{TTIP} = 0.8$, the murky white phenomenon was intensified and the spinning ability got worse. Accordingly, the fiber diameter increased. It was found that the optimum φ_{TTIP} condition for PVAc/TTIP electrospinning was 0.2. As confirmed by TEM analysis, unique core-sheath structures were observed after annealing at 400 and 600°C. XRD data indicated that Ti-deposited TiO_2 nanofibers annealed at 400°C clearly exhibited typical peak at $2\theta = 25.3°$, corresponding to the (101) reflection of TiO_2 anatase crystals. Particularly, Ti-deposited TiO_2 nanofibers annealed at 400°C showed lowest transmission value in the UV region. This derives from the fact that anatase-type has the most outstanding property as a photocatalysis. In addition, Ti-deposited TiO_2 nanofibers annealed at 400°C clearly showed dramatic decrease in formaldehyde gas (deodorizing efficiency ~ 70.7%), which is obviously higher than that (deodorizing efficiency ~ 50.0%) of the same sample annealed at 900°C, indicating that anatase type has more effective photocatalysis performance than rutile type.

This work was supported by the 2008 Yeungnam University Research Grant in 2008 (208-A-235-290).

References

1. Teo, E.; Ramakrishna, S. Nanotechnology 2006, 17, R89.
2. Park, J. C.; Ito, T.; Kim, K. O.; Kim, K. W.; Kim, B. S.; Khil, M. S.; Kim, H. Y.; Kim, I. S. Polym J 2010, 42, 273.
3. Ohsawa, O.; Lee, K. H.; Kim, B. S.; Lee, S.; Kim, I. S. Polymer 2010, 51, 2007.
4. Sato, H.; Kim, K. O.; Kim, H. K.; Kim, B. S.; Enomoto, Y.; Kim, I. S. Fibers Polym 2010, 11, 1123.
5. Kim, C. K.; Kim, B. S.; Sheikh, F. A.; Lee, U. S.; Khil, M. S.; Kim, H. Y. Macromolecules 2007, 40, 4823.
6. Thompson, T. L.; Yates, J. T. Chem Rev 2006, 106, 4428.
7. Ghadiri,E.; Taghavinia, N.; Zakeeruddin, S. M.; Grätzel, M.; Moser, J. E. Nano Lett 2010, 10(5),1632.
8. Fujishima A.; Rao T. N.; Tryk, D. A. J. Photochem Photobiol C: Photochem Rev 2000, 1, 1.
9. Grätzel, M. Nature 2001, 414, 338.
10. Fu, G.; Vary, P. S.; Lin, C. T. J Phys Chem B 2005, 109, 8889.
11. Kawahara, T.; Konishi, Y.; Tada, H.; Tohge, N.; Nishii, J.; Ito, S. Angew Chem Int Ed 2002, 41, 2811.
12. Zhang, J.; Xu, Q.; Feng, Z.; Li, M.; Li, C. Angew Chem Int Ed 2008, 47, 1766.
13. Noguchi, T.; Fujishima, A.; Sawunyama, P.; Hashimoto, K. Environ Sci Technol 1998, 32, 3831.
14. Sunada, K.; Kikuchi, Y.; Hashimoto, K.; Fujishima, A. Environ Sci Technol 1998, 32, 726.
15. Choi, S. K.; Kim, S.; Kim, S. K.; Park, H. J Phys Chem C 2010, 114, 16475.
16. Kumar, A.; Jose, R.; Fujihara, K.; Wang, J.; Ramakrishna, S. Chem Mater 2007, 19, 6536.
17. Kim, I. D.; Rothschild, A.; Lee, B. H.; Kim, D. Y.; Jo, S. M.; Tuller, H. L. Nano Lett 2006, 6, 2009.
18. Sill, T. J.; von Recum, H. A. Biomaterials 2008, 29, 1989.
19. Greiner, A.; Wendorff, J. H. Angew Chem Int Ed 2007, 46, 5670.
20. Schiffman, J. D.; Schauer, C. L. Polym Rev 2008, 48, 317.
21. Christopher, D.; Xin, L.; David, Z.; Xianyan, W.; Ferdinando, F. B.; James, W.; Lynne, A. S.; Jayant, K. Nano Lett 2003, 3, 143.
22. Bognitzki, M.; Hou, H.; Ishaque, M.; Frese, T.; Hellwig, M.; Schwarte, C.; Schaper, A.; Wendorff, J. H.; Greiner, A. Adv Mater 2000, 12, 637.
23. Wei, K.; Ohta, T.; Kim, B. S.; Lee, K. H.; Kim, K. W.; Khil, M. S.; Kim, H. Y.; Kim, I. S. Polym Adv Technol 2009, 21, 746.
24. Kim, H. R.; Ito, T.; Kim, B. S.; Watanabe, Y.; Kim, I. S. Adv Eng Mater 2011, 13, 376.
25. Kimura, N.; Kim, H. K.; Kim, B. S.; Lee, K. H.; Kim, I. S. Macromol Mater Eng 2010, 295, 1090.
26. Wei, K.; Li, Y.; Kim, K. O.; Nakagawa, Y.; Kim, B. S.; Abe, K.; Chen, G. Q.; Kim, I. S. J Biomed Mater Res A 2011, 97, 272.
27. Kim, B. S.; Kim, I. S. Polym Rev, 2011, 51, 235.
28. Zhang, X.; Xu, S.; Han, G. Mater Lett 2009, 63, 1761.
29. Hotovy, I.; Huran, J.; Spiess, L. J Mater Sci 2004, 39, 2609.